VALIDATION OF SLENDERFLOW IN SHIP - SHIP INTERACTION SCENARIOS

ANDREAS VERBEKE, GHENT UNIVERSITY, BELGIUM
TIM GOURLAY, PERTH HYDRO, AUSTRALIA
GUILLAUME DELEFORTRIE, GHENT UNIVERSITY, BELGIUM
MAXIM CANDRIES, GHENT UNIVERSITY, BELGIUM
WIM VAN HOYDONCK, FLANDERS HYDRAULICS, BELGIUM
EVERT LATAIRE, GHENT UNIVERSITY, BELGIUM

SUMMARY

Ship-to-ship interactions can induce significant vertical motions, increasing grounding risks. Experimental data on this phenomenon remain scarce, so numerical methods could provide an alternative to assess these risks. A numerical method based on slender-body theory was implemented by Gourlay (2009), who used a linear superposition of ship-bound pressure fields in open water to calculate ship sinkage and trim during ship-to-ship interactions. A Fourier solution of these pressure fields was implemented in the computer code *SlenderFlow* (SF). In this paper, Gourlay's superposition method was implemented using SF and validated with experimental data obtained at Flanders Hydraulics (FH). The results showed that SF captures qualitative trends, but its predictions underestimate the peak magnitudes of the unsteady sinkages. This discrepancy is attributed to model simplifications, such as the linearization of the hull and free-surface boundary conditions, but also the superposition of separate pressure fields is questioned.

NOMENCLATURE

A_{M}	Surface area of midship section (m^2)
A_{W}	Waterplane area (m^2)
B	Maximum moulded breadth (m)
$\bar{B}(k)$	Fourier transform of $B(x)$ (m^2)
B_{i}	Maximum moulded breadth of ship I (m)
$B(x)$	Ship breadth on the waterline at longitudinal position x(m)
Fr_h	Depth-based Froude number (-)
$Fr_{h,\mathrm{crit1}}$	First critical Froude depth number (-)
$Fr_{h,\mathrm{i}}$	Depth-based Froude number of ship i (-)
g	Gravitational acceleration constant (9.81 m/s^2)
h	Water depth (m)
I_{LCF}	Second moment of waterplane area (m^4)
k	Dimensional wave number (1/m)
$K(k)$	Kernel function determined by canal bathymetries (-)
L	Submerged length of the own ship (m)
$L_{\mathrm{PP,i}}$	Length between perpendiculars of ship i (m)
m	Canal blockage (-)
$p_i(x_j, y_j)$	Pressure field due to ship i in ship-bound reference system of ship j (N/m^2)
U	Free stream velocity (m/s)
U_{i}	Ship speed magnitude of ship i (knots or m/s)
U_{rel}	Relative speed of target vessel w.r.t. own ship (knots or m/s)
s_0	Sinkage at midships (m)
s	Sinkage (m)
s_{AP}	Sinkage at the aft perpendicular (m)
s_{FP}	Sinkage at the fore perpendicular (m)
s_{LCF}	Sinkage at LCF (m)
s_{peak}	Peak magnitude of the unsteady sinkage (m)
s_{steady}	Steady sinkage (m)
$\bar{S}'(k)$	Fourier transform of derivative of $S(x)$ (m^3/m)
$S(x)$	Hull cross-sectional area at station x (m^2)
$S'(x)$	Derivative of hull cross-sectional area at station x (m^2/m)

t	Time (s)
T	Ship draft (m)
T_i	Draft of ship i (m)
w	Canal width (m)
x	Longitudinal coordinate in ship-bound reference system (m)
X	Variable of integration (m)
$\overline{xB}(k)$	Fourier transform of $(x - x_\mathrm{LCF})B(x)$ (m^3)
x_cc	Longitudinal distance between midship sections (m)
x_i	Longitudinal coordinate (in reference system i) (m)
$x_\mathrm{i,LCF}$	Longitudinal coordinate of centre of floatation in reference system of ship i (m)
y	Transverse coordinate in ship-bound reference system (m)
y_cc	Transverse distance between symmetry planes (m)
y_i	Transverse coordinate (in reference system i) (m)
z	Vertical coordinate in ship-bound reference system(m)
z_i	Vertical coordinate (in reference system of ship i) (m)
Z_steady	Steady vertical heave force (positive upwards) (N)
$Z(t)$	Unsteady vertical heave force (positive upwards) as function of time (N)
Z_total	Vertical heave force, sum of steady and unsteady component (N)
θ_LCF	Trim about LCF (radians)
λ	Scale factor (-)
∇	Moulded volume (m^3)
ξ	Stagger distance (-)
ρ	Density of water (kg/m^3)
ϕ	Disturbance velocity potential (m^2/s)
Ω	Cross-section area of the canal (m^2)
Exp	Experiment
FH	Flanders Hydraulics
LCF	Longitudinal centre of floatation
SF	SlenderFlow
UKC	Under Keel Clearance (-)
$_0$	Subscript, indicating the inertial frame of reference2
$_\mathrm{own}$	Subscript, indicating the own ship
$_\mathrm{tar}$	Subscript, indicating the target ship

1 INTRODUCTION

Ships manoeuvring in close proximity generate interaction forces due to overlapping ship-bound pressure fields. With increasing ship sizes, the frequency of interaction-related accidents rises, highlighting the relevance of this issue. This problem is not new and has been the topic of many publications (see Zhou et al. (2023) and references therein). However, the main focus of these investigations lies on the forces acting in the horizontal plane due to the passage of another vessel. The specific problem of vertical motions caused by ship interactions has received comparatively little attention (Gourlay, 2009).

Eloot et al. (2011) pointed out that squat and trim during ship-to-ship interaction play an important role in the design of two-way navigation channels, in which vertical dimensions should be sufficient to account for the additional squat caused by ship-to-ship interactions. However, experimental data on this topic remains scarce. Experimental data was reported by Dand (1981). It was shown that large changes in trim and sinkage can occur, increasing the grounding risk. Vantorre et al. (2002) conducted extensive ship-to-ship interaction tests but did not analyse vertical displacements.

Numerical models offer an alternative to experimental data. Gourlay (2009) applied slender-body theory to calculate ship sinkage and trim during ship interaction using an integral expression from Tuck (1966) to calculate the pressure field of a ship in open water. This approach assumes linear superposition of pressure fields but lacked experimental validation.

The pressure field calculated by Tuck (1966) involves the direct integration of a singular integral. To overcome this singularity, Gourlay (2008) proposed an alternative solution involving a Fourier transform. This Fourier transform solution was implemented in the computer code *SlenderFlow* (SF) (Gourlay, 2008; Ha, 2018). The computer code also incorporates the solution to other bathymetries (Gourlay, 2008). With the ship geometry, velocity and bathymetry as input, SF calculates the hydrodynamic pressure fields, steady sinkage and trim of a single ship.

The goal of this paper is to validate the linear superposition method proposed by Gourlay (2009) with data obtained by Vantorre et al. (2002). Instead of Tuck's integral expression of the pressure field in open water, the Fourier-based solutions presented by Gourlay (2008) are modified to calculate the pressure field of a passing target ship.

The paper first presents the slender-body theory of Tuck and his integral solution. The shortcomings of this solution are explained, after which the alternative solution using Fourier transforms is presented. Then, the solution of the flow field around a ship in a canal of constant width is presented, since validation is performed with model test results obtained in a towing tank of constant width. This bathymetry was also included in SF. Subsequently, the superposition method is explained. Finally, the numerical results are compared to experimental results.

2 THEORETICAL METHOD

2.1 THEORETICAL BACKGROUND OF SLENDERFLOW

The computer code *SlenderFlow* calculates the hydrodynamic pressure fields, steady sinkage and trim of a single ship sailing in different bathymetries. The code assumes the ship-bound coordinate systems as shown in Figure *1*. To explain the theoretical background of SF, consider the own ship with ship-bound coordinate system ($x_{\text{own}}, y_{\text{own}}, z_{\text{own}}$). This coordinate system will be denoted with (x, y, z) in this section for ease of notation.

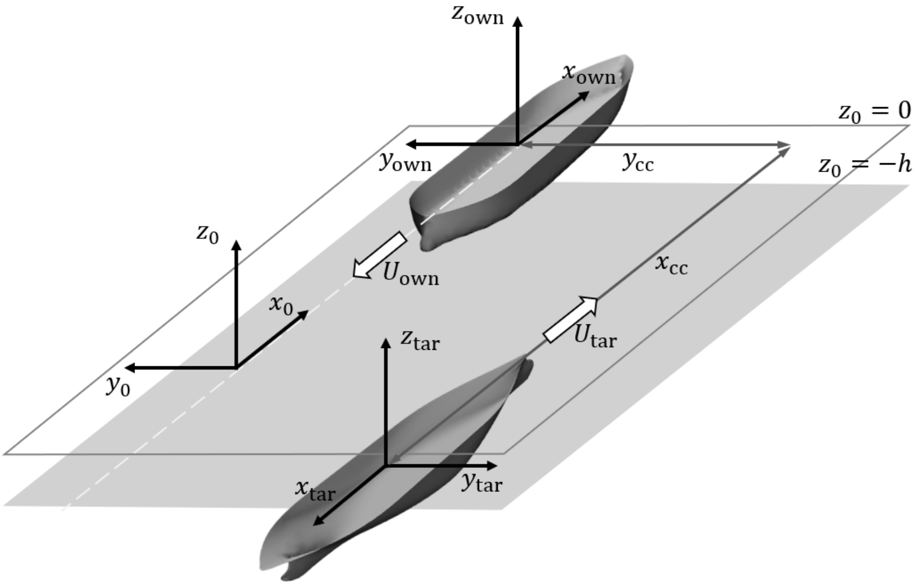

Figure 1 Coordinate systems and notation

The longitudinal coordinate x is centred at midships (positive towards the stern). The transverse coordinate y is centred on the ship's centreline (positive to starboard) and the vertical coordinate z lies at the undisturbed free surface (positive upwards). In this ship-fixed coordinate system, the ship is stationary and is subjected to a steady incoming freestream of magnitude U, which equals the own ship speed U_{own}.

All solutions implemented in *SF* were derived from a partial differential equation derived by Tuck (1966). He derived that the leading order disturbance velocity potential ϕ should satisfy the linearized shallow-water equation in the outer region

$$(1 - Fr_h^2)\frac{\partial^2 \phi}{\partial x^2} + \frac{\partial^2 \phi}{\partial y^2} = 0. \tag{1}$$

Fr_h is the depth-based Froude number ($U/\sqrt{gh}$), with h the water depth. It is subject to a modified linearised hull boundary condition (the inner boundary condition)

$$\frac{\partial\phi}{\partial y} = \pm\frac{U}{2h}S'(x\,) \text{ on } y = 0_{\pm}, \tag{2}$$

where $S(x)$ is the hull cross-sectional area at station x and $S'(x)$ is the derivative of this section area with respect to x. According to linear theory the ship is fixed in its rest position when calculating the flow, so the increase of the immersed volume due to sinkage is neglected when calculating $S(x)$ in Eq. (*2*) (Gourlay, 2008).

Depending on the specific bathymetry, additional boundary conditions are introduced. For open water of constant depth, Eq. (*1*) is subject to the far-field boundary condition

$$\frac{\partial\phi}{\partial x}, \frac{\partial\phi}{\partial y} \to 0 \text{ as } y \to \pm\infty. \tag{3}$$

In a canal of constant depth h and canal width w, with the ship sailing at the canal centreline, a wall boundary condition at the sides of the canal is introduced (Tuck, 1967):

$$\frac{\partial\phi}{\partial y} = 0 \text{ on } y = \pm\frac{w}{2}. \tag{4}$$

Other bathymetries require additional details (Gourlay, 2008).

The velocity potential can be calculated from the elliptic partial differential equation ($Fr_h < 1$) Eq. (*1*) by considering the boundary conditions. This potential can then be employed to derive the hydrodynamic pressure. This pressure is given from the linearized Bernoulli equation as (Gourlay, 2014)

$$p(x, y) = -\rho U\frac{\partial\phi}{\partial x}. \tag{5}$$

Higher-order (quadratic) terms are neglected in the Bernoulli equation, since these are of the same order as other terms already neglected in the derivation of the linearized shallow-water equation Eq. (*1*) and hull boundary condition Eq. (*2*) (Gourlay, 2014).

Tuck (1966) solved this boundary value problem for the case of a ship sailing in open water by considering the velocity potential for a line of moving sources (Gourlay, 2008). The pressure field around this ship moving at a steady velocity U is equal to

$$p(x, y) = -\frac{\rho U^2}{2\pi h\sqrt{1 - Fr_h^2}}\int_{-\frac{L}{2}}^{\frac{L}{2}}\frac{x - X}{(x - X)^2 + (1 - Fr_h^2)y^2}\,\frac{dS}{dX}\,dX, \tag{6}$$

In Eq. (*6*) X represents the variable of integration along the length of the ship. L is the submerged length of the ship and equals the distance between the foremost and aftmost point.

For locations away from the ship's centreline ($y \neq 0$), the integrand in Eq. (*6*) is non-singular and the integral may be evaluated using Simpson's rule (Gourlay, 2014). Additionally, the singularity at y = 0 is integrable except right at the bow or stern where $S'(x)$ is discontinuous.

To address this issue, (Gourlay, 2008) proposed an alternative solution which uses Fourier transforms rather than source summations, which was implemented in SF (Ha, 2018). The pressure field surrounding a ship in open water of constant depth may be written as

$$p(x, y) = -\frac{\rho U^2}{4\pi h\sqrt{1 - Fr_h^2}}\int_{-\infty}^{\infty} i\,\mathrm{sgn}(k)\overline{S'}(k)\,e^{-\sqrt{1-Fr_h^2}|k||y|}e^{-ikx}dk. \tag{7}$$

The real part of Eq. (7) is considered for physical quantities. The Fourier transform of the derivative of the section area $\overline{S'}(k)$ is calculated directly as (Gourlay, 2014)

$$\overline{S'}(k) = \int_{-\infty}^{\infty}\frac{dS}{dx}e^{ikx}dx. \tag{8}$$

Since this integral is highly oscillatory for large values of $|k|$, Filon's method is employed to evaluate this integral. This Fourier transform does not quite tend to zero as $|k| \to \infty$, due to the discontinuities in $S'(x)$ at the bow and stern. Consequently, the singularity at the bow and stern remains in Eq. (7), but the singularity at other locations on the hull ($y = 0$) is lifted, allowing the use of Simpson's rule.

The expression for the pressure Eq. (7) can be generalized to other bathymetries as

$$p(x,y) = -\frac{\rho U^2}{4\pi h\sqrt{1-Fr_h^2}}\int_{-\infty}^{\infty} i\,K(k)\bar{S}'(k)\,e^{-\sqrt{1-Fr_h^2}|k||y|}e^{-ikx}dk. \tag{9}$$

The function $K(k)$ depends on the transverse geometry (Gourlay, 2008). For instance, in open water

$$K(k) = \operatorname{sgn}(k), \tag{10}$$

which can be derived from Eq. (7). In a rectangular canal

$$K(k) = \coth\left(\left(\frac{W}{2}\right)\sqrt{1-Fr_h^2 k}\right). \tag{11}$$

The pressure on the hull $p(x, 0)$ can be used to calculate the vertical heave force Z and bow-down trim moment about the longitudinal centre of floatation (LCF) M_{LCF} to first order (Tuck, 1966). Using the slender-body approximation, these are calculated as

$$Z = \int_{-L/2}^{L/2} p(x,0)B(x)\,dx = -\frac{\rho U^2}{4\pi h\sqrt{1-Fr_h^2}}\int_{-\infty}^{+\infty} i\bar{S}'(k)\overline{B^*}(k)K(k)dk, \tag{12}$$

$$M_{LCF} = \int_{-\frac{L}{2}}^{\frac{L}{2}} p(x,0)B(x)\,(x - x_{LCF})dx = -\frac{\rho U^2}{4\pi h\sqrt{1-Fr_h^2}}\int_{-\infty}^{+\infty} i\bar{S}'(k)\overline{xB^*}(k)K(k)dk. \tag{13}$$

$\bar{B}(k)$ denotes the Fourier transform of $B(x)$. The asterisk denotes the complex conjugate. $\overline{xB}(k)$ is the Fourier transform of $(x - x_{\mathrm{LCF}})B(x)$. SlenderFlow includes additional bathymetries, such as a dredged and stepped canal. More details can be found in (Gourlay, 2008).

The upwards vertical force Z is related to the sinkage of the LCF s_{LCF}. and waterplane area A_{W} through hydrostatic balancing via (Gourlay, 2009)

$$Z = -\rho g A_{\mathrm{w}} s_{\mathrm{LCF}}. \tag{14}$$

Similarly, the steady bow-down trim θ_{LCF}(in radians) is related to the bow-down moment through

$$M_{\mathrm{LCF}} = \rho g I_{\mathrm{LCF}}\theta_{\mathrm{LCF}}, \tag{15}$$

$$I_{\mathrm{LCF}} = \int_{-L/2}^{L/2} (X - x_{\mathrm{LCF}})B(X)dX. \tag{16}$$

x_{LCF} is the coordinate of the longitudinal centre of floatation in the ship-bound reference system.

It is clear that a number of assumptions are made when developing the code. Firstly, the slender-body is based on the potential flow assumptions, so boundary layer thickening along the hull is absent. This is especially important at model scale, where the boundary layer is thicker and more likely to separate, increasing the difference in results between experiments and SF results. Additionally, the absence of self-propulsion in SF, might aggravate these effects.

The water depth is small compared to the ship's length, so vertical velocities are assumed to be much smaller than horizontal flow components. Consequently, the flow is essentially horizontal.

Finally, both the free-surface and hull boundary conditions are linearized. The linear solution uses only the leading-order dynamic free surface boundary conditions, assuming free surface displacements to be small (Gourlay, 2008). Hull-boundary conditions are linearized by assuming that the ship's beam is much smaller than its length. Neglecting these non-linearities are especially important for fuller ship shapes, such as bulk carriers and tankers.

2.2 SHIP INTERACTION WITH SLENDERFLOW

The calculation of sinkages due to ship interaction is based on Gourlay (2009). The unsteady sinkage of a ship (called the own ship) due to a passing ship (called the target ship) was calculated via linear superposition of the pressure fields attached to the own and target ship. Each of these pressure fields is calculated as if the ship were sailing alone in the canal (section 2.1), so unsteady effects, related to the passing ship, are neglected according to this method.This linear superposition was based on Yeung (1978), who found analytically that the dominant heave force and pitch moment were due to linear superposition of the pressure fields produced by each ship (Gourlay, 2009).

The examples studies in this paper consider two ships sailing along parallel trajectories (Figure *1*). It was assumed that the distance between both ships $y_{\mathrm{cc}}$is large compared to each ship's beam and of similar order to each ship's length. In this way, each ship lies entirely in the far field of the other vessel. A ship-fixed coordinate system is attached to the own ship ($x_{\mathrm{own}}, y_{\mathrm{own}}, z_{own}$) and the target ship ($x_{\mathrm{tar}}, y_{\mathrm{tar}}, z_{\mathrm{tar}}$). The own ship and target ship have a constant forward velocity of U_{own} and U_{tar} respectively. An earth-fixed reference frame is introduced as well (x_0, y_0, z_0). The y_0-coordinate is chosen such that the centreline of the own ship lies on $y_0 = 0$. The centreline of the target vessel lies on $y_0 = y_{\mathrm{cc}}$. The (x_0, t) coordinates are chosen such that the submerged midships of both ships pass through $x_0 = 0$ at time $t = 0$.

With the coordinate systems in Figure 1, Gourlay's (2009) approach is applied. The superposed pressure on the own vessel consists of two terms. The first term is the pressure due to the own ship, which is calculated by taking $y = 0$in Eq.(9). The second term is the pressure due to the target ship on the own ship. It is found by expressing the target ship-bound pressure field $p_{\mathrm{tar}}(x_{\mathrm{tar}}, y_{\mathrm{tar}})$ in the coordinate system $(x_{\mathrm{own}}, y_{\mathrm{own}})$. For an encounter manoeuvre $x_{\mathrm{tar}} = -x_{\mathrm{own}} + (U_{\mathrm{own}} + U_{\mathrm{tar}})t = -x_{\mathrm{own}} + x_{\mathrm{cc}}$. It follows that, if t is negative before the encounter manoeuvre, x_{cc} is negative when both ships are approaching and positive once both ships have passed each other. Similarly, $y_{\mathrm{tar}} = -y_{\mathrm{own}} + y_{\mathrm{cc}}$, where y_{cc} is negative in Figure 1. This results in the pressure acting on the own ship, due to an encountering target ship, by taking $y_{\mathrm{own}} = 0$in the following expression,

$$p_{\mathrm{tar}}(x_{\mathrm{own}}, y_{\mathrm{own}}, t) = -\frac{\rho U_{\mathrm{tar}}^2}{4\pi h\sqrt{1 - Fr_{h,\mathrm{tar}}^2}} \int_{-\infty}^{\infty} i\, K(k)\overline{S_{\mathrm{tar}}'}(k)\, e^{-\sqrt{1-Fr_{h,\mathrm{tar}}^2}|k||y_{\mathrm{cc}}-y_{\mathrm{own}}|} e^{-ik(-x_{\mathrm{own}}+x_{\mathrm{cc}}(t))} dk, \tag{17}$$

where $Fr_{h,\mathrm{tar}} = U_{\mathrm{tar}}/\sqrt{gh}$. This pressure can be integrated over the own ship to obtain the unsteady sinkage force:

$$Z(t) = \int_{-\frac{L}{2}}^{\frac{L}{2}} p_{\mathrm{tar}}(x, 0, t) B(x)\, dx. \tag{18}$$

This integration is performed numerically to evaluate the unsteady sinkage term. The unsteady trim moment is found by replacing $B(x)$ with $(x - x_{\mathrm{LCF}})B(x)$ in Eq. (*18*). The total vertical force on the own vessel during the encounter manoeuvre is calculated as

$$Z_{\mathrm{total}} = Z_{\mathrm{steady}} + Z(t), \tag{19}$$

where Z_{steady} is calculated with Eq. (*12*).

Similarly, the pressure field of a target ship when overtaking a slower own ship becomes

$$p_{\mathrm{tar}}(x_{\mathrm{own}}, y_{\mathrm{own}}, t) = -\frac{\rho U_{\mathrm{tar}}^2}{4\pi h\sqrt{1 - Fr_{h,\mathrm{tar}}^2}} \int_{-\infty}^{\infty} i\, sgn(k)\overline{S'}(k)\, e^{-\sqrt{1-Fr_{h,\mathrm{tar}}^2}|k||y_{\mathrm{own}}-y_{\mathrm{cc}}|} e^{-ik(x_{\mathrm{own}}+x_{\mathrm{cc}}(t))} dk, \tag{20}$$

where $x_{\mathrm{cc}} = (U_{\mathrm{tar}} - U_{\mathrm{own}})t$. Since t is negative before the target ship overtakes the own ship, x_{cc} is negative before the overtaking manoeuvre and positive once the target ship has passed the own ship.

With the total vertical force and moment, the total sinkage and trim angle can be calculated again via Eq. (*14*) and Eq. (*15*), since it was shown through a dynamic motion analysis that changes in sinkage and trim are sufficiently slow for a quasi-steady method to be employed (Gourlay, 2009).

The unsteady interaction phenomenon is simplified considerably with this approach, as proposed by (Gourlay, 2009). In essence, the unsteadiness only arises through the fact that the ship-bound coordinate systems are moving in space with respect to each other. After all, the interaction is approximated as a superposition of two pressure fields. Each of these ship-bound pressure fields is calculated as if the ship is sailing alone through a canal. The pressure fields were calculated using a linearized Bernoulli equations which neglected the time derivative of the potential. Therefore, the effect of unsteadiness is greatly simplified in the current approach.

3 EXPERIMENTAL DATA

3.1 EXPERIMENTAL PROGRAM

The SF results will be compared to a selection of experimental results obtained by Vantorre et al. (2002). They provided a summary of the ship-ship test program performed in the Towing Tank for Manoeuvres in Confined Water at FH, as well as a description of the test setup and tested parameters. The lines plans of all 4 tested ship models are given in Fig. 3 (from Vantorre et al., 2002).

A selection of experiments was made, which included only three of the 4 tested ship models. The dimensions and drafts of these ships are presented in Table *1* at model scale and full scale. The scale factor λ equals 75. Ship E (T0E)[1] and ship H (T0H) are both used as own vessel in the validation. In each test, the own vessel was fitted with a propeller and rudder and each test was executed at the model self-propulsion point. T0E is a large tanker, while T0H is a smaller tanker. T0E and ship D (C0D) are used as target vessel. No propeller or rudder was fitted to the target ship. C0D is a container ship of similar length as T0 E, but with a smaller width.

Table 1. Dimensions of ship models

	Model scale			Full scale (λ=75)		
Ship code	T0E	T0H	C0D	T0E	T0H	C0D
L_{PP} (m)	3.824	2.211	3.864	286.8	165.8	289.8
B (m)	0.624	0.296	0.536	46.80	22.20	40.25
T (m)	0.207	0.178	0.180	15.53	13.35	13.50
∇ (m^3)	0.4029	0.0989	0.2914	169 981	41 706	92 578

SF requires knowledge on the precise hull geometry. Two offset files are created for each ship (at a specific draft) containing the breadth on the waterline at every station $B(x)$ and the submerged cross section at each station $S(x)$ respectively. The geometry of the ship models is used to generate the offset files. The section area $S(x)$ and half ship width is given in Figure 2.

Both encounters and overtaking scenarios are included in the validation. Only overtaking scenarios where the own ship is being overtaken are considered, since these scenarios result in stronger interaction forces compared to the cases where the own ship overtakes a target vessel. An overview of tested parameters was provided in Table *2*.

[1] D,E,H are the ship codes used by Vantorre et al. (2002). Nowadays, FH uses the codes C0D, T0E and T0H for these ship models respectively. These codes are also used in the remainder of the paper.

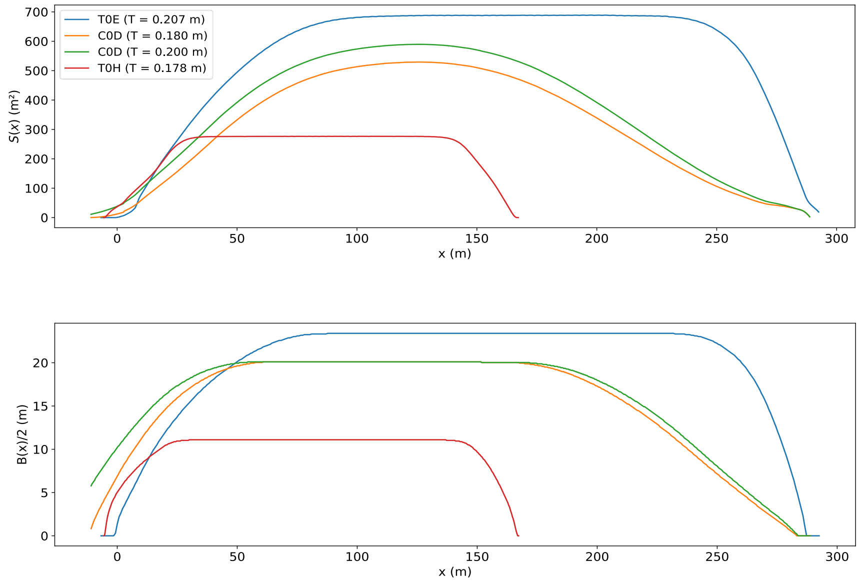

Figure 2 Submerged cross-section area at each station $S(x)$ (top figure) and half width at the waterline at each station $B(x)/2$ (bottom figure). $S(x)$ and $B(x)$ are inputted in SF. The aft perpendicular lies at x=0.

Table 2. Parameters included in the validation study (at model scale). The ship code of the own vessel is given in y_{cc}/B_{own} column.

Manoeuvre	U_{own}(m/s)	U_{tar} (m/s)	$y_{\mathrm{cc}}/B_{\mathrm{i}}$ (-)		h (m)
			T0E	T0H	
Encounter	0.238	0.475	1.2	*2.1*	0.228
Overtaking ($U_{\mathrm{tar}} > U_{\mathrm{own}}$)	0.475	0.713	1.4	*3.7*	0.248
		0.950	1.9	*4.6*	0.307
			2.8	*5.6*	
				6.6	

3.2 SINKAGE MEASUREMENTS

The vertical displacements at four positions (fore/aft; port/starboard) are measured during the model tests. Measurements were only taken on the own vessel attached to the main carriage. These measurements are converted to the vertical displacements at three locations: at the fore perpendicular s_{FP}, at midships s_0 and at the aft perpendicular s_{AP}.

The measurements corresponding to an encounter and overtaking manoeuvre are shown in Figure 3 and Figure 4 respectively. Only the forces on the own vessel (T0E) are given. These are plotted against the non-dimensional stagger distance calculated as

$$\xi = \frac{x_{\mathrm{cc}}}{\frac{1}{2}\left(L_{\mathrm{PP,own}} + L_{\mathrm{PP,tar}}\right)}. \tag{21}$$

In this expression, $x_{cc}$is the longitudinal distance between midship sections (Figure 1) and L_{PP} refers to the length between perpendiculars. Given the definition of x_{cc} in section 2.2, ξ is negative before the passing and positive after. During an encounter, the bows of both ships pass at ξ =-1. The sterns of both ships are aligned when $\xi = 1$. When the own ship is overtaken, ξ =-1 when the bow of the target ship passes the stern of the own ship. Conversely, ξ =1 when the stern of the target ship passes the bow of the own ship. $\xi = 0$ when the midship sections cross. All model test results are scaled to full scale. Scaling is achieved by multiplying the measured sinkage with the scale factor ($\lambda = 75$).

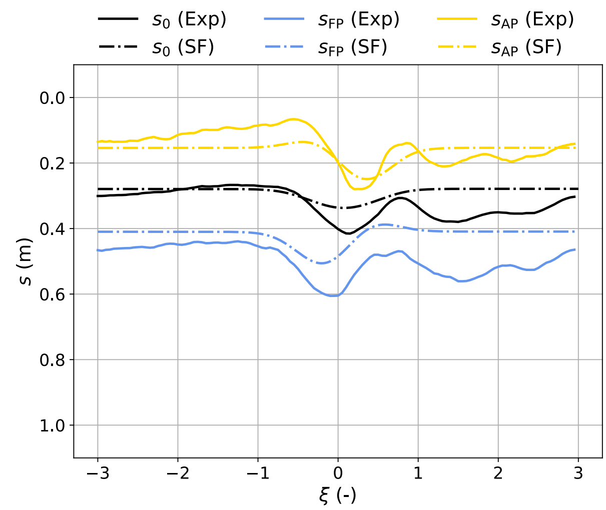

Figure 4 Comparison between sinkages calculated with SF and experimental results amidhips (s_0), at the fore perpendicular (s_{FP}) and at the aft perpendicular (s_{AP}). Encounter of T0E (own ship) and C0D (target ship), both sailing at 8 knots, Fr_h =0.305, h = 18.6 m and y_{cc} = 131 m.

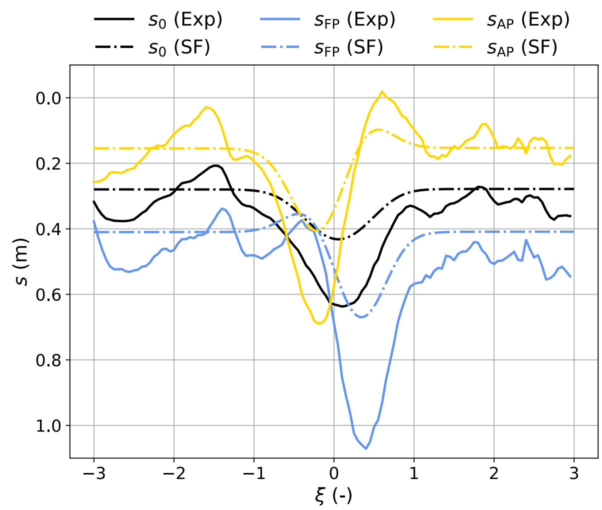

Figure 3 Comparison between sinkages calculated with)SF and experimental results at the fore perpendicular (s_0), at the fore perpendicular (s_{FP}) and at the aft perpendicular (s_{AP}). T0E (own ship sailing at 8 knots, Fr_h = 0.305) is overtaken by C0D (target ship, sailing at 12 knots, Fr_h=0.457), h = 18.6 m, y_{cc} = 131 m.

In contrast with the experiments, SF calculates the sinkage of the LCF s_{LCF} and the bow-down trim angle θ_{LCF} (Eq. (*15*) and Eq. (*16*) respectively). These values were combined to calculate the sinkages at the three experimental locations:

$$s_{\mathrm{FP}} = s_{\mathrm{LCF}} + \left(\frac{1}{2} L_{\mathrm{PP,own}} + x_{\mathrm{LCF}}\right) \cdot \tan\left(\theta_{\mathrm{LCF}}\right) \tag{22}$$

$$s_{\mathrm{AP}} = s_{\mathrm{LCF}} - \left(\frac{1}{2} L_{\mathrm{PP,own}} - x_{\mathrm{LCF}}\right) \cdot \tan\left(\theta_{\mathrm{LCF}}\right) \tag{23}$$

$$s_0 = s_{\mathrm{LCF}} + x_{\mathrm{LCF}} \cdot \tan\left(\theta_{\mathrm{LCF}}\right) \tag{24}$$

Both s_{LCF} and θ_{LCF} consist of a steady sinkage value caused by the own ship's movement through the water, and an unsteady contribution due to the passing ship.

4 COMPARISON OF SLENDERFLOW WITH MODEL TESTS

4.1 METHODOLOGY

Experimentally obtained trendlines are compared to SF trendlines in Figure 3 and Figure 4. Three sinkages are investigated: s_0, s_{FP} and s_{AP}. These sinkages consists of two contributions: a steady sinkage, corresponding to a single ship sailing through a canal and an unsteady sinkage, corresponding to the passing target ship.

The performance of SF when calculating steady sinkages was discussed before (Gourlay, 2014). SF tended to underestimate the average sinkage and overestimate the bow-down trim when compared to model tests, primarily due to the linearization of the free surface (Gourlay, 2008). The overestimation of the bow-down trim corresponds to under-estimating $s_{\mathrm{AP}}$and over-estimating s_{FP}. However, this observation was not confirmed by Figure 3, since the propulsion and flow separation near the stern in the experiments decreases the bow-down trim.

In general, SF succeeds to predict some qualitative trends present in the experimental results. Firstly, Figure 3 and Figure 4 show that the sinkage near the aft s_{AP} is smaller than the sinkage at the bow $s_{\mathrm{FP},}$ both in the experiments and SF. This bow-down trim is typical for tankers, which have a large part of their volume in the fore part of the ship (Figure 2). Container ships usually show a bow-up moment (Eloot et al., 2011). Secondly, the number and location of peaks in the sinkage trend is predicted reasonably well by SF. The midship sinkage s_0 predicts a single peak near ξ=0. The sinkages at the bow and stern s_{FP} and s_{AP} predict a smaller peak and a larger peak. Lastly, both the experiments and SF show larger interaction peak magnitudes during an overtaking manoeuvre than during the encounter.

On the other hand, differences are observed as well. The main differences are the peak magnitudes and the fact that the experimental measurements show additional oscillations, which are related to the interaction of the Kelvin wave patterns.

Given these differences between the theoretical and experimental results, the validation will be limited to a comparison of peak magnitudes of the unsteady sinkage. After all, this maximum peak magnitude is the most important part of the sinkage analysis. The unsteady part is obtained by deducting the steady sinkage from the total sinkage trend line. This is straightforward for the SF result. For the experimental results, a steady state value was calculated by computing the average sinkage over the range $\xi = -3$ and $\xi = -2.5$. The maximum value of the unsteady trend line is determined and compared in the next sections.

4.2 INFLUENCE OF SEPARATION

The experimental program tested a range of lateral separations. However, the focus of the experimental test program was on close ship passings, so the maximal full-scale y_{cc} equalled 131 m. Theoretically, SF cannot be used to replicate these tests, since the target vessel is not entirely in the far field of the own vessel. Since the separations were larger than the own ship's breadth, it was assumed that the theory is approximately valid.

Figure 5 compares the experimental peak magnitudes with the unsteady SF peaks. Overall, it is clear that both for encountering and overtaking, the peak magnitudes decrease as y_{cc} increases. This decrease is more pronounced for the experimental peaks, so the comparison between experiment and software improves as the separation increases. In general however, the SF peak is an underestimation of the actual peak. This suggest that the target ship's water level depression amidships is underestimated in SF, which could be due to the linearisation of the hull and free surface boundary condition.

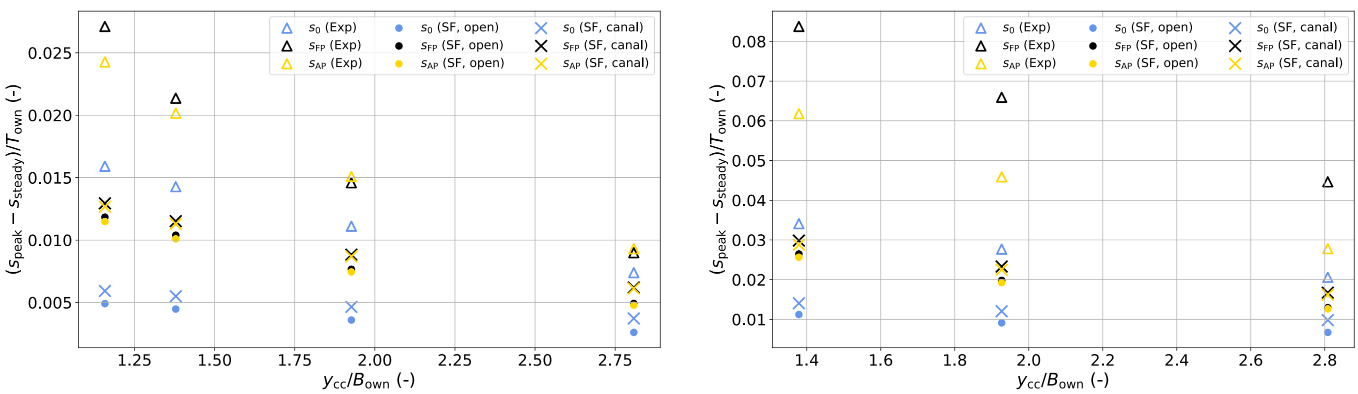

Figure 5 Influence of separation on the interaction peak size. Left: Large tanker T0E (own ship) and large container ship C0D (target ship) encounter at equal speed (8 knots) in a water depth of 18.6 m. Right: Large container ship C0D (target ship), sailing 12 knots, overtakes large tanker T0E (own ship), sailing 8 knots, in a water depth of 18.6 m. The legend indicates whether the pressure field of the target ship was calculated with an 'open' or 'canal' bathymetry.

Additionally, it was investigated whether the target ship's pressure field should be computed using an open water or canal bathymetry. Gourlay (2009) stated that for ships in a canal with reasonable width, the single ship flows as calculated by SF can be linearly superimposed to describe the total flow around two ships travelling on parallel courses. However, a single ship flow, corresponding to a ship in a canal, assumes that the ship sails along the centre line. In Figure 6 both ships were resolved in a canal bathymetry. Clearly, the pressure field due to the container ship is not physically possible near the wall. However, since the canal geometry results in a larger pressure close to this container ship, the interaction peak magnitudes increase slightly over the entire range of y_{cc}, improving the comparison between experiment and SF.

It is concluded that, even though using a canal bathymetry for the target ship results in a non-physical pressure field, the proposed superposition of single canal flows is useful as long as the own ship is not sailing through this zone with incorrect pressure prediction. This is the case when the canal is wide enough.

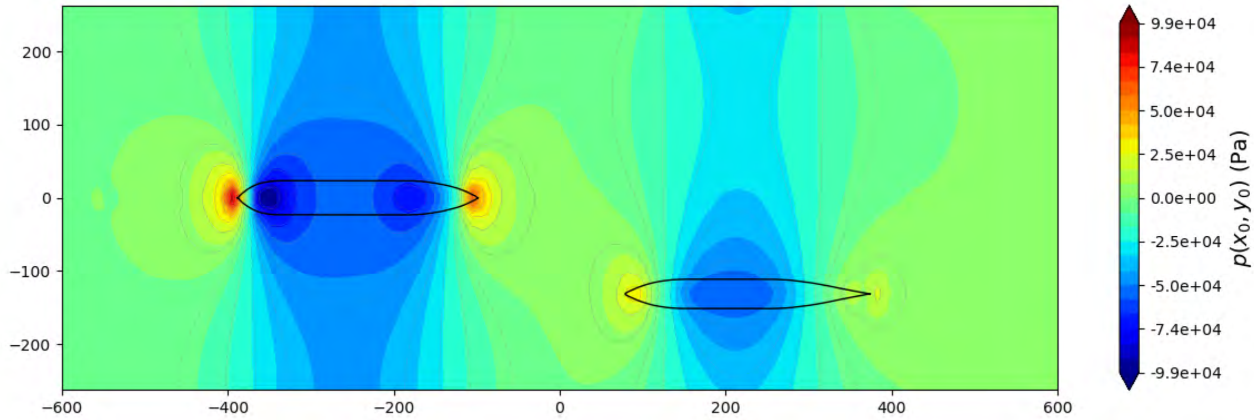

Figure 6 Pressure field after an encounter manoeuvre. Large tanker T0E (sailing to the left) encountered the large container ship C0D (sailing to the right) at equal velocities of 8 knots in a canal of 525 m (= $\lambda \cdot w$). The pressure fields are calculated assuming a canal bathymetry, assuming each ship lies on the centreline of the respective canal.

4.3 INFLUENCE OF UKC

For 20% UKC (calculated as $(h - T_{\text{own}})/T_{\text{own}}$) and 50% UKC of the own ship, similar observations are made as before: the SF interaction peaks underpredict the actual peak sizes, but as the UKC increases the peak magnitudes decrease, improving the prediction. The sinkage at the bow s_{FP} is also larger than the peak sinkage at the stern s_{AP}.

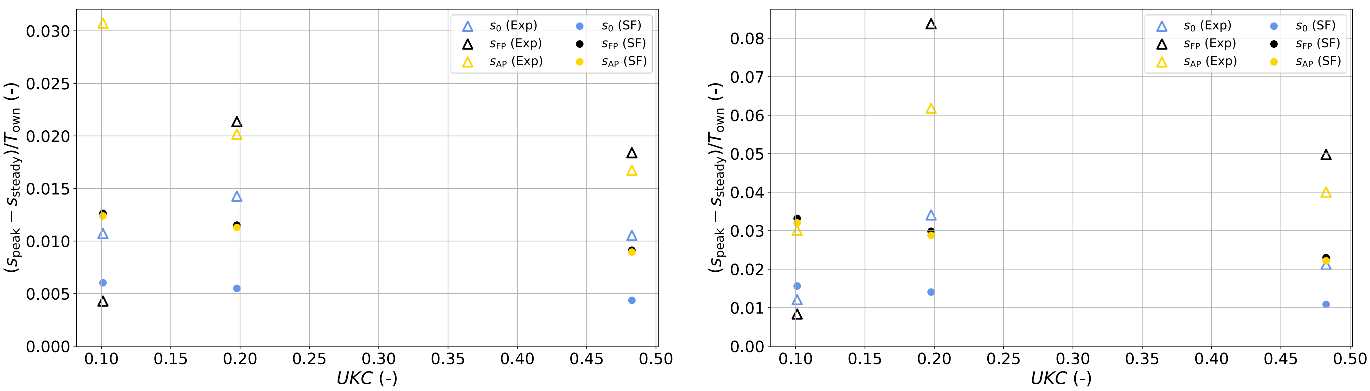

Figure 7 Influence of the UKC (of the own ship) on the interaction peak size. Left: Large tanker T0E (own ship) and large container ship C0D (target ship) encounter at equal speed (8 knots) with a lateral separation y_{cc} = 64.5 m. Right: Large container ship C0D (target ship), sailing 12 knots, overtakes large tanker T0E (own ship), sailing 8 knots, with a lateral separation y_{cc} = 64.5 m.

At a small UKC of 10%, the experimental sinkages deviate from the general pattern. At this UKC, the water flow beneath the keel is blocked, reducing the sinkage at the bow, while the sinkage aft is influenced by low pressure zone created by the propeller action (Eloot et al., 2011). Additionally, the trim of the own ship, and thus the sinkages s_{FP} and s_{AP}, depends simultaneously on the pressure near the forward and aft shoulders. These pressures depend in turn on the longitudinal volume and waterplane area of both ships sailing in shallow water (Gourlay, 2014). Further research is required to understand the combined effect of these observations on the experimentally determined interaction peaks.

In contrast to the experiments, the sinkages calculated with SF increase steadily with decreasing UKC. The UKC does not appear explicitly in the calculation of the unsteady vertical force, rather through the water depth h and the ship section distribution $S(x)$. Consequently, differences are expected between theoretical results and model test results at very small UKC.

4.4 INFLUENCE OF VELOCITY

Both the velocity of the own and target ship determine to great extent the interaction forces. In Figure 8 the interaction peaks obtained with SF and experiments during encounter manoeuvres at different speeds are compared. The relative speed is calculated as U_{rel} = U_{tar}-U_{own}, where $U_{\mathrm{own}}$is a negative value for the encounter manoeuvre. Three speed combinations are considered (U_{own} -U_{tar}): 4 knots – 8 knots; 8 knots – 8 knots; 8 knots – 12 knots.
The experimental peaks increase with increasing U_{rel}, even when the target ship speed remains constant. The theoretical peaks increase at well, but the SF peaks at 12 knots and 16 knots are identical. Clearly, in Eq. (*17*) and Eq. (20), the unsteady vertical force only depends on the speed of the passing vessel. This implies that the superposition of pressure fields as investigated in this paper was an oversimplification.

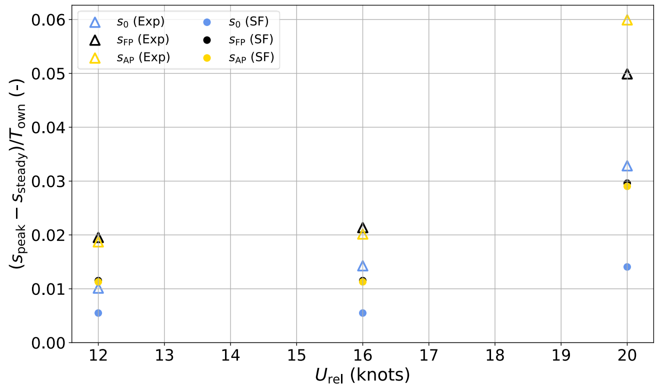

Figure 8 Influence of relative velocity on the interaction peak size. Large tanker T0E (own ship) and large container ship C0D (target ship) encounter in water of depth h = 18.6 m with a lateral separation y_{cc} = 64.5 m.

4.5 INFLUENCE OF SHIP SHAPE

The results presented so far were limited to the interaction between a large tanker (T0E, own ship) and container ship (C0D, target ship) of similar length. However, the ship shapes have an important effect on the pressure fields. When calculating the unsteady interaction, the hull shape of the target ship appears in Eq. (*17*) and Eq. (20). The length and waterplane of the own vessel influence the sinkage values via Eq. (*22*) through (*24*).

To verify the effect of the hull shape, both the interaction between a smaller tanker (T0H) and a large tanker (T0E) and between a smaller tanker (T0H) and large container ship (C0D) was investigated (Figure 9). The smaller tanker is the own ship. The influence of y_{cc} is very comparable to the result of Figure 5. By comparing the results of Figure 9 with those of Figure 5, the effect of the own shape ship is assessed. The interaction between the small tanker and the container ship shows smaller s_{FP} and s_{AP} peaks (experimentally) than the interaction between the large tanker and the container ship. The shorter length of T0H seems an important reason. SF on the other hand predicts larger s_{FP} and s_{AP} peaks for the interaction between the small tanker and container ship as compared to the interaction between the large tanker and container ship. Further examination into this issue is required.

Figure 9 also includes the interaction peaks corresponding to the interaction between a smaller tanker and a large tanker. The large container ship is wider and has a longer parallel midship than the large container ship (Figure 2). When changing the target ship, all peaks (experimental and theoretical) increase. The longer parallel midship causes a greater sinkage of the water level compared to the container ship (Eloot et al., 2011), which increases the interaction sinkage. The increase of interactions peak when changing the container ship with a large tanker is relatively larger for the experiments, which again indicates that the pressure field predicted by SF is underestimated because the free-surface and hull boundary conditions are linearized.

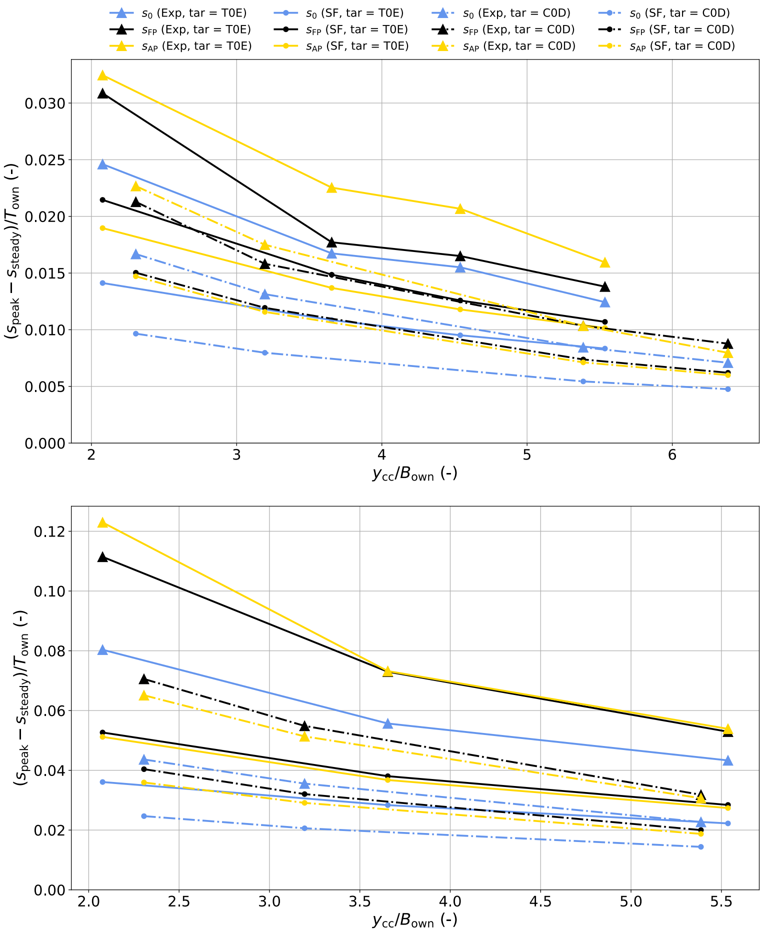

Figure 9 Influence of the hull shape and lateral separation on the interaction peak size. Top figure: Encounter of small tanker T0H (own ship) with large tanker T0E (target ship) (solid line) or large container ship C0D (target ship) (dashed line). Both ships are sailing at 8 knots in a water depth of 18.6 m. Bottom figure: Small tanker T0H (own ship) is overtaken by a large tanker T0E (target ship) (solid line) or large container ship C0D (target ship) (dashed line). T0H is sailing at 8 knots, while the target ships is sailing at 12 knots at h = 18.6 m.

4.6 INFLUENCE OF PROBLEM FORMULATION

All solutions implemented in SF were derived starting from the partial differential equation proposed by Tuck (1966). These solutions have a singularity as Fr_h approaches 1, which corresponds to a transition from subcritical to trans-critical flow. Gourlay (2000) attributed the failing of the basic shallow-water theory close to Fr_h = 1 to the neglect of dispersive effects. By modifying the shallow-water theory to include dispersive effects in open water, the sinkage at transcritical Froude numbers could be calculated.

However, ships such as bulk carriers displace water in confined waters, which has to return along the hull. At some combinations of ship speed and canal confinement, the water can no longer be evacuated along the ship's hull, resulting in a pile-up in front of the vessel. This speed is also known as the first critical speed and it is shown by Delefortrie et al. (2024) that this critical speed depends on the blockage m of the canal:

$$Fr_{h,\mathrm{crit1}} = \left(2\sin\left[\frac{\arcsin(1-m)}{3}\right]\right)^{3/2}. \qquad (25)$$

Here is m the blockage factor, calculated as A_{M}/Ω. A_{M} is the surface area of the midship section and Ω is the total cross-section area of the canal. This expression is commonly attributed to Schijf (1949), although he only presented a formula for the critical blockage without showing expressions for the critical speed (Delefortrie et al., 2024).

In case of a target container ship (C0D) moving in the towing tank, A_{M} = 589.59 m^2, Ω=9765 m^2, m =0.0604 and the critical water depth dependent Froude number equals 0.705. Comparing this to a critical Fr_h=1 in open water, it could be concluded that the shallow-water continuity equation Eq. (*1*) overestimates the critical velocity in case of confined channels.

To test the influence of the critical speed, the shallow-water equation Eq. (*1*) was, without mathematical derivation, re-written to

$$\left(Fr_{h,\mathrm{crit1}}^2 - Fr_h^2\right)\frac{\partial^2\phi}{\partial x^2} + \frac{\partial^2\phi}{\partial y^2} = 0. \tag{26}$$

Since $Fr_{h,\mathrm{crit1}}$ is not dependent on x or y, re-deriving Eq. (*17*) in a canal of constant width results in

$$p_{\mathrm{tar}}(x_{\mathrm{own}}, y_{\mathrm{own}}, t) = -\frac{\rho U_{\mathrm{tar}}^2}{4\pi h\sqrt{Fr_{h,\mathrm{crit1}}^2 - Fr_{h,\mathrm{tar}}^2}}\int_{-\infty}^{\infty} i\,K(k)\overline{S_{\mathrm{tar}}'}(k)\,e^{-\sqrt{Fr_{h,\mathrm{crit1}}^2 - Fr_{h,\mathrm{tar}}^2}|k||y_{\mathrm{cc}} - y_{\mathrm{own}}|}e^{-ik(-x_{\mathrm{own}} + x_{\mathrm{cc}}(t))}dk, \tag{27}$$

$$K(k) = \coth\left(\left(\frac{W}{2}\right)\sqrt{Fr_{h,\mathrm{crit1}}^2 - Fr_{h,\mathrm{tar}}^2}\,k\right). \tag{28}$$

The interaction peaks during an encounter manoeuvre of the large tanker T0E and large container ship C0D, as function of the lateral separation, are shown in Figure 10. The reformulated SF solution improves the peak magnitudes at smaller separations. However, the reformulated SF solution decreases less with y_{cc}, resulting in an overestimation of the interaction peaks at larger separation distances. It should be kept in mind that Eq. (1) was developed for a single ship in open water. The current correction only addressed the confinement of the canal. However, the unsteady effect, due to the presence of another ship, is still simplified according to this correction. A new slender-body shallow water equation should be derived, which considers the (moving) target ship.

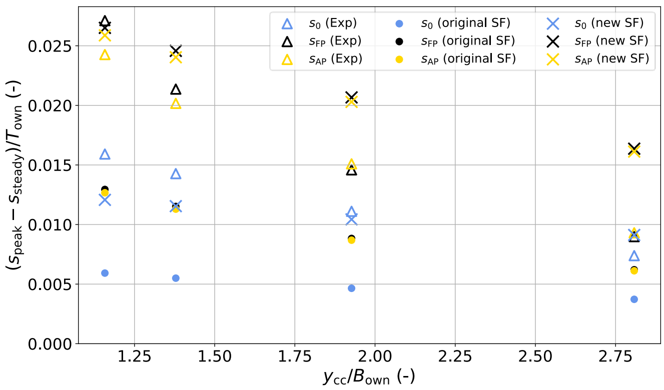

Figure 10 Influence of the lateral separation on the interaction peak size. Tanker E and container ship D encounter at equal speed (8 knots) in a water depth of 18.6 m. Three results are compared: interaction peak sizes of the experiments, interaction peak sizes solved with the original boundary value problem (original SF) and interaction peak sizes solved with the reformulated boundary value problem (new SF).

5 CONCLUSIONS

Significant changes in trim and sinkage can occur when two ships pass in a narrow canal, increasing the risk of grounding. Despite this risk and the high frequency of ship interactions in port areas, limited experimental data exists on vertical ship motions during such interactions. A method was presented by Gourlay (2009) involving the superposition of ship-bound pressure fields to estimate these effects. However, due to lack of experimental data, the accuracy of this approach remained uncertain.

This paper implements Gourlay's method via the *SlenderFlow* (SF) computer code, which uses Fourier transforms to calculate the ship-bound pressure field. An unsteady sinkage could be calculated via the pressure field attached to the target ship and was validated against experimental data.

SF accurately predicts qualitative characteristics of the trend lines, such as the location and number of peaks. Additionally, overtaking manoeuvres induce larger interaction effects than encounter manoeuvres both in the experiments and SF calculations. Also, the distribution of volume in the ship is included correctly.

The qualitative effect of separation y_{cc}, UKC and relative speed is predicted correctly in some cases. For instance, reducing the lateral separation increases sinkages both in the experiments and calculations. On the other hand, SF predicts monotonically increasing sinkages with decreasing UKC or increasing relative velocity, while this is contradicted by the experimental results.

SF systematically underestimates unsteady peak sinkages. Its predictions improve when interaction forces are low, such as at lower speeds, larger separation distances, or greater under-keel clearance (UKC).The underprediction of the interaction sinkages by SF is both related to the simplifications of the theoretical model and the superposition assumption. The main simplifications used in the theory include: ignoring self-propulsion effects, neglecting boundary layer thickening (especially during model tests), linearization of the hull boundary condition and linearization of the free surface condition (Gourlay, 2014). Since these limitations influence the pressure field of the target vessel, the sinkage due to interaction will also be affected by these limitations. For instance, linearization of the hull boundary condition and free-surface result in an underprediction of the low pressure zone amidship of the target vessel, especially for bulky ships such as tankers. This implies that the drawdown force on the own ship due to the passage of a target ship is larger in the experiments, resulting in larger experimental sinkages. Propulsion effects and boundary layer thickening decrease the pressure near the stern during the experiment, further influencing the pressure field.

It was also shown that the superposition method is an oversimplification. After all, the sinkage of the own vessel, due to the passing of a target ship, increases the submerged volume of the own ship. This in turn will influence the own ship's pressure field, resulting in larger experimental sinkages. This effect depends on different parameters such as the separation and ship velocities. Additionally, a target ship is an obstruction for the water flow around the own ship, which will in turn influence the pressure field of the own ship. Lastly, the proposed superposition method ignores unsteady effects, which also contributes to the difference between experimental and numerical results.

Additional investigations into the use of SF for assessing ship interactions are required. Firstly, the comparison in this paper was between the theoretical method and scaled model test results. However, at model scale (low Reynolds number), the boundary layer is thick compared to the ship's dimensions and more likely to separate near the stern, which may markedly change the hull pressure near the stern (Gourlay, 2008). At full scale the boundary layer is thinner and exerts less influence on the hull. Therefore, it is expected that the flow characteristics at full scale better resemble the potential flow assumption used in the theoretical method. Comparison with full-scale results could therefore prove useful.

Secondly, SF results under-predicted the experimental results. It could be investigated whether a correction factor can be found, depending on relevant parameters, to enhance the prediction by SF*.* However, reformulating the boundary value problem showed an improvement for smaller separations, so it should also be investigated under what conditions the mathematical basis remains valid. Also the lack of unsteadiness in the current method deserves further attention.

Lastly, a superposition of two single flows in a specific bathymetry was used in this paper. It was illustrated that this approach leads to unphysical pressure fields, since it is assumed that a ship sails along the canal's centre line when calculating the pressure field. A cross-flow should be included in the theoretical model to extend the approach to ships sailing off-centre.

6 REFERENCES

Dand, I.W., 1981. Some measurements of interaction between ship models passing on parallel courses, in: National Maritime Institute. National Maritime Inst., Feltham, pp. 1–92.

Delefortrie, G., Verwilligen, J., Vantorre, M., Lataire, E., 2024. Exact and Approximated Solutions to the Critical Ship Speeds in Canals, in: Schoonhees, J.S. (Ed.), Proceedings of the 35th PIANC World Congress 2024. PIANC, Capetown, South Africa, pp. 649–654.

Eloot, K., Vantorre, M., Verwilligen, J., Prins, H., Hasselaar, T.W.F., Mesuere, M., 2011. Squat during ship-to-ship interactions in shallow water, in: Pettersen, B., Berg, T.E., Eloot, K, Vantorre, M (Eds.), Proceedings of the 2nd International Conference on Ship Manoeuvring in Shallow and Confined Water (MASHCON), 18 - 20 May 2011, Trondheim, Norway. R.I.N.A, pp. 117–126.

Gourlay, T., 2014. ShallowFlow: A Program to Model Ship Hydrodynamics in Shallow Water, in: OMAE 2014. San Francisco, USA, p. V01AT01A018.

Gourlay, T., 2009. Sinkage and trim of two ships passing each other on parallel courses. Ocean Eng. 36, 1119–1127. https://doi.org/10.1016/j.oceaneng.2009.06.003

Gourlay, T., 2008. Slender-body methods for predicting ship squat. Ocean Eng. 35, 191–200. https://doi.org/10.1016/j.oceaneng.2007.09.001

Gourlay, T., 2000. Mathematical and Computational Techniques for Predicting the Squat of Ships. The University of Adelaide, Adelaide, Australia.

Ha, J.H., 2018. Measurement and Simulation of Ship Under-Keel Clearance in Port Approach Channels. PhD Thesis. Centre for Marine Science and Technology, Curtin University.

Schijf, J.B., 1949. Protection of Embankments and Bed in Inland and Maritime Waters, and in Overflow or Weirs, in: XVII International Navigation Congress, Lisbon, Section I. pp. 61–78.

Tuck, E.O., 1967. Sinkage and trim in shallow water of finite width. Schiffstechnik 73, 92–94.

Tuck, E.O., 1966. Shallow-Water Flows Past Slender Bodies. J. Fluid Mech. 26, 81–95.

Vantorre, M., Verzhbitskaya, E., Laforce, E., 2002. Model test based formulations of ship-ship interaction forces. Sh. Technol. Res. 49, 124–141.

Yeung, R.W., 1978. On the interactions of slender ships in shallow water. J. Fluid Mech. 85, 143–159.

Zhou, J., Ren, J., Bai, W., 2023. Survey on hydrodynamic analysis of ship–ship interaction during the past decade. Ocean Eng. 278, 114361. https://doi.org/10.1016/J.OCEANENG.2023.114361

7 AUTHORS BIOGRAPHY

Andreas Verbeke, mechanical engineer, is a PhD researcher at the Ships and Marine Technology Division at Ghent University, Belgium. His research focuses on the development of an improved real-time model to calculate hydrodynamic ship-to-ship interaction in 6 degrees of freedom. The model is to be implemented in the ship simulators at Flanders Hydraulics.

Tim Gourlay is a mathematician specializing in ship hydrodynamics. Through his company, Perth Hydro, Tim undertakes consulting work in ship manoeuvring, seakeeping, under-keel clearance and dynamic mooring.

Guillaume Delefortrie: naval architect (MSc, Ghent University 2001, PhD, Ghent University, 2007), associate professor at the Ships and Marine Technology Division of Ghent University, lecturer in charge of courses in marine hydrodynamics. Experienced in EFD based research, with focus point on ship manoeuvring in shallow and confined water. He has been a member of the 27*th*-29*th* ITTC Manoeuvring Committee. Member of the organization and scientific committees of MASHCON conferences since their creation (2009).

Maxim Candries is a postdoctoral researcher at the Ships and Marine Technology Division of Ghent University.

Wim Van Hoydonck obtained his PhD at Delft University of Technology and is nautical researcher at Flanders Hydraulics. His research interests include the application of numerical methods to ship hydrodynamics and aerodynamics.

Evert Lataire is head of the Ships and Marine Technology Division at Ghent University. His research focuses on the behaviour of ships in shallow and confined waters and is often based on model tests. In recent years his division diversified to other floating devices subject to waves and current such as aquaculture in open sea and floating PV-panels in an offshore environment. Member of the organization and scientific committees of all MASHCON conferences .